IEEE Access
Multidisciplinary | Rapid Review | Open Access Journal

Received November 23, 2020, accepted December 3, 2020, date of publication December 9, 2020,
date of current version December 18, 2020.

Digital Object Identifier 10.1109/ACCESS.2020.3043432

Electromagnetic Performance of the Novel Hybrid-Pole Permanent Magnet Machines for High Peak Torque Density

YU-XI LIU[1], JI-WEI CAO[2], (Member, IEEE), QIN-HE GAO[1], ZHI-HAO LIU[1], YA-CHAO LU[3], AND ZHI-YIN SUN[2], (Member, IEEE)

[1]Institute of Armament Launch Theory and Technology, Xi'an Research Institute of High Technology, Xi'an 710025, China
[2]Department of Electrical Engineering, Harbin Institute of Technology, Harbin 150001, China
[3]Department of Electrical Engineering, Xi'an Institute of Optics and Precision Mechanics of CAS, Xi'an 710119, China

Corresponding author: Qin-He Gao (849852677@qq.com)

This work was supported in part by the National Natural Science Foundation of China under Grant 51877053, in part by the Young Scientists Fund of the National Natural Science Foundation of China under Grant 51807039, in part by the research supported by the National Natural Science Foundation of China under Grant 51905541, in part by the Natural Science Basic Research Plan in Shaanxi Province of China under Grant 2020JQ487, and in part by the Young Talent Fund of University Association for Science and Technology in Shaanxi under Grant 20190412.

ABSTRACT This paper proposes two novel hybrid rotors permanent magnet (PM) machines for the high torque density in short duration condition operation. In order to enhance the torque performance, the flux concentrated structure of spoke-type PM is employed to increase the air-gap flux density. Meanwhile, the non-magnetic connector of the rotor is employed to eliminate the magnetic flux leakage. The rotors of the conventional machines and the proposed machines are optimized by the finite element analysis (FEA). Furthermore, based on the comparisons of electromagnetic performances for the optimized machines, including the open-circuit flux density, torque, PM eddy current loss, overload capability, the characteristics of the proposed machines are analyzed. The results indicate that the proposed machine can improve the torque at rated and overload operation with growth rate 14.3% and 13.1%, respectively. Finally, a 12-slots/10-pole PM machine is prototyped and FEA is to be validated.

INDEX TERMS Hybrid rotors, torque density, magnetic flux leakage, overload capability.

I. INTRODUCTION

Permanent magnet machines have been widely used in the aerospace industry and electric vehicles field all over the world owing to the excellent performance, such as high-power density, high reliability and high efficiency [1]–[4]. Meanwhile, the high torque density is commonly required in direct drive servo system for high performance in industrial robot application and steering gear. The high peak torque density is important electromagnetic indicator which is closely related to the overload capability due to the high dynamic response with a short-time operation. In actual, a low inertia torque is expected by reducing the moment of inertia as small as possible in the rotor outer diameter [5].

The associate editor coordinating the review of this manuscript and approving it for publication was Canbing Li.

It is important to improve the torque performance effectively including the peak torque by using the topologies and reasonable optimization. In [6], the characteristics of the PM and the torque are analyzed by increasing the thickness and width of the PM for the same volume but with different shapes. The results show that it is more effective for the torque density by increasing the PM thickness than the width. In [7]–[10] , the spoke type PM machines are employed to improve torque because of the flux concentrated structure which it can increase magnetic flux emitting area of IPMSMs from the larger magnet surface area. The analytical methods of the spoke-type PM machines are built with the not ideal boundary conditions and irregular geometric model [11]. In [12]–[14], the magnetic bridges are equivalent to fan-shaped saturation regions and the trapezoid magnet is simplified to sector magnets to achieve accurate prediction. In [15], A rotor shaping technique with optimal third

harmonic, which is into the rotor outer surface shape, is presented to enhance the average torque of interior permanent-magnet (IPM) machines. The optimal value has been derived and further confirmed by both finite-element analyses and experiments.

The reduction of the leakage flux around the rotor inner circumference is important issues for the spoke type IPM machine. The shaft with nonmagnetic materials can reduce the flux leakage effectively in spite of a complicate manufacturing process [7], [16], [17]. Another approach is that the magnetic bridge structure is employed with a narrow width of the iron ribs, which structural strength needs to be challenged [18], [19]. In [20], a novel step-staggered rotor with alternated airspace barriers is proposed to reduce the leakage flux around the rotor inner circumference.

Moreover, the machines with consequent pole and hybrid pole PM rotor are employed to increase the torque density and PM utilization [21]. The tangential PMs are embedded into the rotors yoke which is equivalent to an increase in assistant flux [22]. In [23], a comparison of typical V shape, ∇ shape, and $\nabla + U$ shape IPM machines is investigated in the torque density, torque ripple, etc. What is more, the overload capability of the SPM and IPM machines is analyzed. The result shows the SPM machine exhibits better overload capability due to the lower magnetic saturation effects with its larger effective air gap [24]. In [25]–[27], a machine with high peak torque density is designed for MIT cheetah robot with 810 g of weight and 30 Nm of torque. Each consisting of short duration large torque commands. followed by periods of lesser torque requirement. The ratio between maximum torque and rated torque is approximately 10:1 with large gap diameter.

In this paper, two novel hybrid PM machines are proposed to improve the torque density, especially the peak torque density in short duration operation. An optimization is achieved for the conventional and proposed machines. Then, the comparisons of electromagnetic performances in four type machines are analyzed. In Section II, the topology structure machines are described. The characteristic of the short duration machines is analyzed with considering the core saturation. In Section III, optimization and analysis of the different rotor shapes are achieved and presented, respectively. In Section IV, comparisons and evaluation of electromagnetic performances are obtained. In Section V, the 12slot/10 pole PM proposed machine are prototyped to validate the FEA analyses. Finally, the conclusion will be derived in Section VI.

II. PM MACHINE WITH DIFFERENT ROTORS

A. TOPOLOGIES

The 12-slots/10-pole PM machine with fractional slot concentrated winding is adopted to investigate the performance of the machine with five different rotors as Fig. 1 (a). Fig. 1 (a) shows the stator structure with 12 slots and winding distribution. It is worthy that all the investigated machines have the same stator for a more objective comparison. Fig. 1 (b) shows the conventional surface-mount PM (SPM) rotor. Fig. 1 (c) and Fig. 1 (d) show the conventional V shape IPM (VIPM) and U shape IPM (UIPM) rotors, respectively. Fig. 1 (e) shows the proposed spliced hybrid rotor PM machines with the non-magnetic connector (SHRPM). Whereas Fig. 1 (f) shows hybrid rotor PM machines with the magnetic bridge structure (BHRPM).

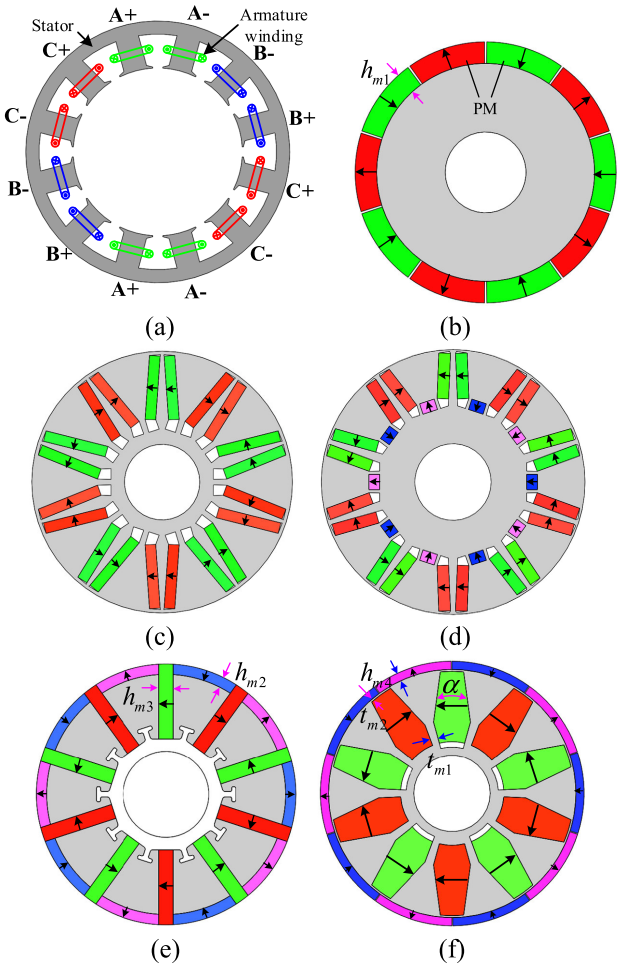

FIGURE 1. Cross sections of different type rotors (a) Stator of 12slots with fractional slot concentrated winding (b) SPM rotor (c) The conventional VIPM rotor (d) The conventional UIPM rotor (e) The proposed SHRPM rotor (f) The proposed BHRPM rotor.

TABLE 1. The main PM machine parameters.

Quantity	Value and unit
Number of pole-pairs	5
Number of stator slots	12
Rated speed	1500rpm
Rated current	20A
Magnet remanence	1.3T
Armature effective length	100mm
Radius of the stator outer surface	39mm
Radius of the stator inner surface	25mm
Number of turns per phase	48
Tooth width	6.9mm

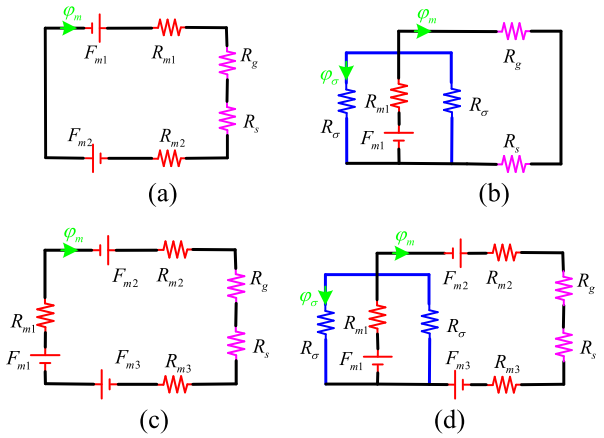

FIGURE 2. Simplified magnetic circuit of four machines (a) SPM machine (b) VIPM machine (c) SHRPM machine (d) BHRPM machine.

B. ELECTROMAGNETIC MODEL ANALYSIS

Fig. 2 show the simplified magnetic circuits (SMC) of machine. R_g and R_s are the equivalent reluctances of the airgap and stator, respectively. R_σ is the leakage reluctance. R_{mi} and F_{mi} are the reluctances and magnetomotive force (MMF) of PMs, which i represent 1, 2 and 3, respectively. Although the rotor outer diameter is the same, magnetic flux area per-pole A_{pm} and magnetization direction length L_{pm} of each pair pole, are different, which are generated by PM.

IPM of spoke type can adopt magnetic circuit in parallel which can increase the magnetic flux area per-pole A_{pm}, but the magnetization direction length L_{pm} will be halved [28]. However, SPM is exactly the opposite due to the PM space layout difference. So, the BHRPM is proposed to take advantage of both effectively as shown in Fig. 2 (d).

Moreover, the reluctance torque will be fully utilized in V shape and U shape IPM, which the SMC is shown as Fig. 2 (b). From it, flux leakage closely related to the magnetic bridge can't be ignored. So, in order to improve the torque density, SHRPM machine will be proposed to limit magnetic bridge leakage based on the BHRPM machine. The corresponding SMC is shown as Fig. 2 (c).

C. ANALYSIS OF THE CORE SATURATION

The core saturation is the important cause of the reduction of the torque coefficient which can restrict the overload capability of the machine. Fig. 3 show the influence of the core saturation on the main magnetic flux with the three different PM layout methods. The line λ_n and λ_l are the linear permeance curve with considering nonlinearity and neglecting it of the core, respectively. $\Delta\Phi_m$ represents the declination of the flux between two PM operating point. The blue line represents new PM recoil curve at different PM shape.

As shown in Fig. 3 (a), the slope of the blue line will less than the primary slope. And ones of the Fig. 3 (b) is the opposite. This shows that the core saturation has a less impact

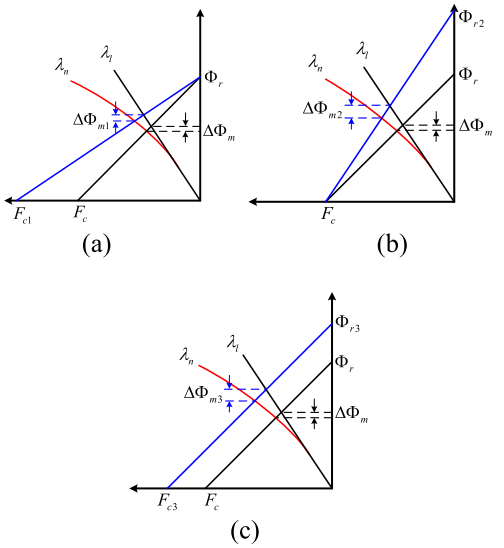

FIGURE 3. Influence of core saturation on the main flux Φ_m in equivalence process with three PM layout methods (a) Increasing thickness of PM (b) Increasing the surface area of PM (c) Increasing the thickness and the surface area of PM.

by increasing the thickness of the PM than by increasing the surface area of PM simply, that is $\Delta\Phi_{m1} < \Delta\Phi_{m2}$.

The MMF of the airgap which is close to the output torque can expressed by

$$F_g = \frac{R_g}{R_s + R_g + R_m} F_m \tag{1}$$

$$\frac{F_{gk}}{F_g} = \frac{R_g + R_s + R_m}{(R_g + R_s)/k + R_m} \tag{2}$$

where F_m represents the MMF of PM. R_m represents the reluctance of all PMs. F_g represents the MMF of the airgap. F_{gk} represent the MMF of the airgap with k times PM's thickness.

From (1), it can indicate that when R_s become bigger (it means more severe core saturation), the influence of the R_m on the F_g will be smaller. Also, the slope will gradually become smaller as shown in Fig. 3 in red line λ_n. It means that when more severe core saturation, the benefit of increasing PM's thickness or the surface area of PM on air-gap magnetic density becomes decreasing. On the other hand, it can be analyzed that when R_m is relatively small, the core saturation is very sensitive to the magnitude of the MMF of air-gap, which also can be shown as the Fig. 3 (b) due to a relatively large slope compared with the Fig. 3 (a). Therefore, torque coefficient will have a greater change as the armature reaction increases. From (2), the air gap magnetomotive force MMF cannot be increased linearly with the thickness of the PM.

The proposed hybrid pole rotor machine can own more flexible variables parameter under limited rotor space by using different combinations of PM which can achieve different electromagnetic performance. Flux concentrated structure

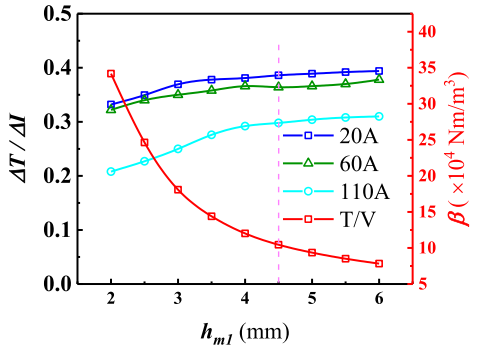

FIGURE 4. The variation of the torque change rate in different current and the volume of the PM with the thickness of the PM for SPM machine.

of spoke-type can also be taken advantage effectively as shown in Fig. 3 (c).

III. OPTIMIZATION WITH DIFFERENT ROTORS

The same rotor outer diameter and sinusoidal current is employed. The control mode is maximum torque per ampere (MTPA) for the optimized machines.

A. SPM

As mention previously, the thickness of PM is key parameter for SPM when the PM-arc ratio is close to 1. In order to investigate the capability of the output torque under different current and the influence of the saturation, torque change rate based on current is defined as

$$\frac{\Delta T}{\Delta i} = \frac{T(i+\Delta i) - T(i)}{\Delta i} \tag{3}$$

where Δi represents a micro-element current, $\Delta T/\Delta I$ represents the torque output capability in unit current at a certain current i. Fig. 4 shows the variations of torque change rate and PM utilization ratio β (the ratio of torque to PM volume) with PM thickness h_{m1} in SPM. It can be seen that $\Delta T/\Delta I$ is increased and the PM utilization ratio β is decreased as h_{m1}, respectively. The growth degree of $\Delta T/\Delta I$ becomes relatively smaller as h_{m1}. This phenomenon can be consistent with the principle explained by the (2). Simultaneously, $\Delta T/\Delta I$ is decreased significantly when the current amplitude is 110A compared with 60A or 20A, especially at a low h_{m1}. This means that larger thickness of PM is more effective on the torque at overload working operation than rated ones. From above, the thickness of PM h_{m1} is chosen as 4.5mm that the result is a trade-off between output torque and PM utilization.

B. THE IPM OF V AND U

Four classic IPM rotor structures, (namely, V shape, V- shape, U shape, and U- shape) are adopted to improve the torque density as shown in Fig. 5. V shape and U shape rotors are optimized by using the FEA software with the parameter variables. V- shape is added '–'shape based on V shape. U- shape is the same. The main parameters are shown as Table 2.

TABLE 2. The key parameters for four IPM rotor structures.

Items	Values	Items	Values
t_1 (mm)	2	b_1 (mm)	1
t_2 (mm)	2	b_2 (mm)	0.6
t_3 (mm)	2.1	b_3 (mm)	0.5
t_4 (mm)	2	b_4 (mm)	0.6
t_5 (mm)	1.3	b_5 (mm)	0.4
θ_1 (°)	22	θ_2 (°)	20

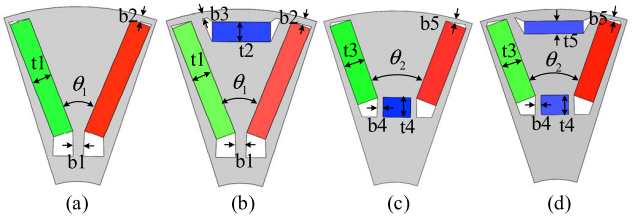

FIGURE 5. Cross sections of one pole for different IPM rotors (a) V type (b) V- type (c) U type (d) U- type.

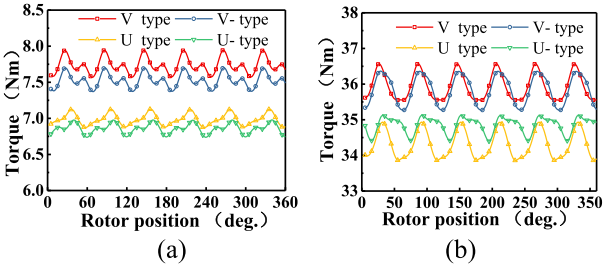

FIGURE 6. The variation of the torque with rotor position for four conventional IPM machines.

Fig. 6 shows the variations of torque with rotor position at rated current (20A) and overload current (110A) in four conventional IPM machines. It can be observed that the torque output of V shape rotor is 7.8Nm and 36.1Nm, which is biggest when the currents are 20A and 110A, respectively. Instead, its torque ripple is greater than the U shape and U- shape. It is worth noting that the torque of U- shape have a larger torque than that of U shape when the current is 110A which is the opposite of the 20A. The reason is that equivalent PM thickness of U- shape is increased to improve the working operation of PM in overload condition. In contrast, the '–' shape and magnetic barrier structure can impede the magnetic flux through the rotor in low current density condition. In addition, the law is applied to that of the V shape and V- shape which is not so relatively significant. Therefore, the optimization V shape rotor machine is determined to investigate the performance in Section 4.

C. BHRPM

The key parameter of the BHRPM rotor is the thickness of surface-mount PM and spoke type PM [5]. In fact, the spoke type is designed as shown in Fig. 1 (f) to reduce the magnetic bridge width for lower the leakage. Then the angle α is employed to weigh the equivalent thickness of this part.

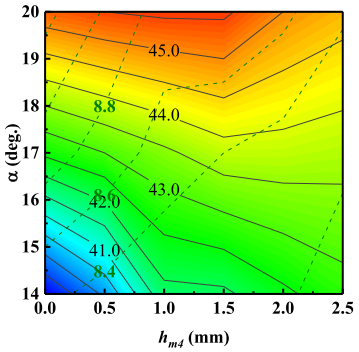

FIGURE 7. The variations of torque and the volume of the PM with parameters h_{m4} and angle at overload current 110A.

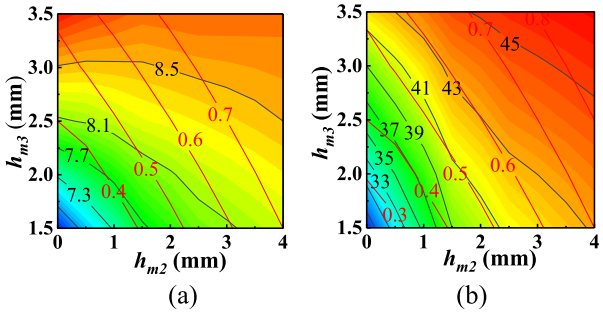

FIGURE 8. The variations of torque and the volume of the PM with parameters h_{m2} and h_{m3} (a) Rated current 20A (b) Overload current 110A.

Fig. 7 shows the variations of torque with parameters h_{m4} and angle α at overload current (110A). The dotted line represents the change in the contour of the PM volume. It is indicated that with the relatively larger angle, the electromagnetic torque achieves more optimized when the thickness of surface-mount PM is designed as 1.5mm. This is because that the thickness of surface mount PM and width of the spoke PM is mutually affected at limit rotor space. The air-gap magnetic density variety with the magnetic source parameters. From above, for sake of the overload capability, the angle is 19.6° and the thickness is 1.5mm. The output torque can reach 45.5Nm in spite of a large amount of PM (8.68×10^{-4}m^3).

D. SHRPM

The main principle of the SHRPM rotor is basically similar to the BHRPM rotor. The non-magnetic connector is employed to connect and fix the segments cores and PMs. Meanwhile, magnetic flux leakage in the PM's bottom is effectively eliminated [28].

Fig. 8 (a) and Fig. 8 (b) show the variations of torque with two parameters (h_{m2} and h_{m3}) at rated and overload current, respectively. The red line represents the distribution in the contour of the PM volume. From Fig. 8 (a), the effect of the torque increased is more obvious by increasing the thickness of the spoke type h_{m3} than surface-mount PM h_{m2} due to a larger slope. Moreover, gradient of the contour line becomes significantly smaller when the torque is more than 43Nm as shown in Fig. 8 (b), which means that the PM utilization ratio is significantly decrease. Based on above analysis and the size of the non-magnetic connector, the thickness of the surface-mount PM and spoke type PM are designed as 1.9 mm and 2.7 mm, respectively.

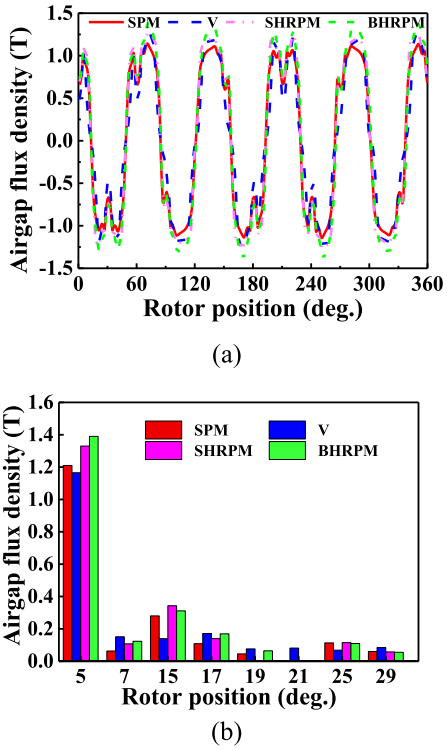

FIGURE 9. The open-circuit air-gap flux density of the four machines (a) Waveforms (b) Harmonics.

IV. COMPARISONS AND EVALUATION OF ELECTROMAGNETIC PERFORMANCE

In the previous section, the key parameters of the four types rotors are optimized by using the FEA when the stator parameters and the armature current is consistent. In order to investigate the electromagnetic performance of the proposed machine (BHRPM and SHRPM), the comparisons will be evaluated compared with the conventional SPM and IPM machine.

A. COMPARISON OF OPEN-CIRCUIT FLUX DENSITY AND HARMONIC

Fig. 9 (a) shows the open-circuit airgap flux density of four different rotors. Obviously, the airgap density amplitude of the proposed BHRPM rotor is largest for all these machines. V shape and SHRPM have almost equal magnitude in airgap density. Fig. 9 (b) shows the corresponding airgap density harmonic distribution. It can be observed that BHRPM and SHRPM rotors own a highest and second highest fundamental amplitude magnetic density (5th). The values are 1.39 T and 1.33 T, respectively, which is exceeded the value of the PM's remanence. This is because that there is a magnetic flux concentrated role in spoke type part due to the larger flux emitting area compared with the airgap area. However,

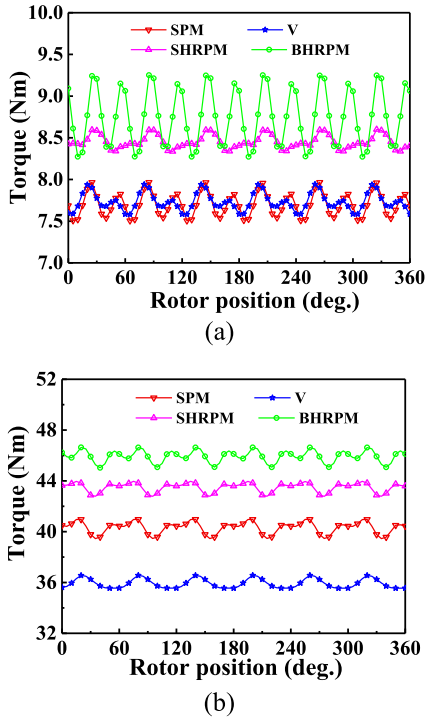

FIGURE 10. The variation of the torque with rotor position for the conventional and proposed machines (a) Rated current 20A (b) Overload current 110A.

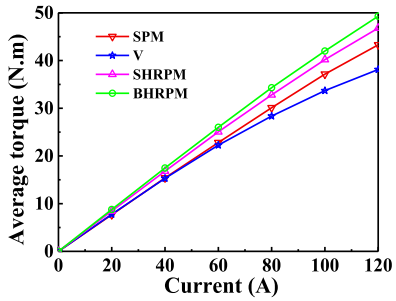

FIGURE 11. The variation of the average torque with the current for the conventional and proposed machines.

the fundamental harmonic content of the SPM is higher than V shape which is contrary to the comparison of the airgap density amplitude. This is due to a small polar arc coefficient for V shape rotor.

B. COMPARISON OF THE TORQUE CHARACTERISTIC

Fig. 10 (a) and Fig. 10 (b) show the variation of the electromagnetic torque for four type machines at rated operation and overload operation, respectively. As shown in Fig. 10 (a), the torque of the conventional SPM and V type machines are 7.65 Nm and 7.75 Nm when the current is 20A. Meanwhile, the torque of the proposed SHRPM and BHRPM machines are 8.45 Nm and 8.75 Nm, respectively. The growth rates are 10.5% and 14.3% compared with the SPM. From Fig. 10 (b), the average torques are 40.5 Nm, 36.0 Nm, 43.5 Nm, and 45.8 Nm when the current is 110A. The growth rates of the proposed machines are 7.4% and 13.1%, respectively. It is

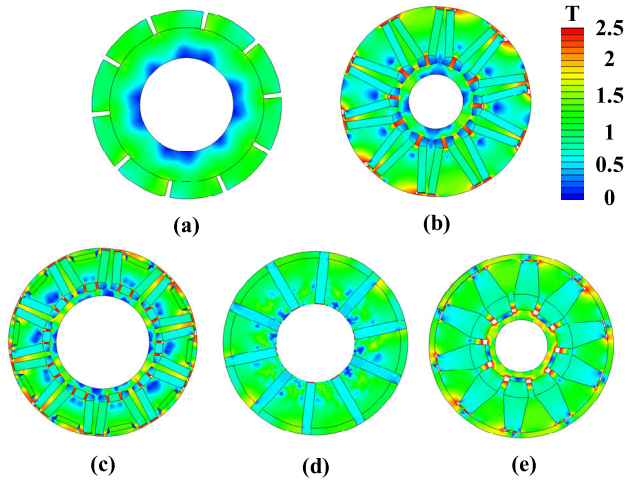

FIGURE 12. Flux density distribution of rotor with different structures when the current is 110A.

well worth to be noted that the torque of the SPM is far greater than V shape which is very different at the rated operation. The reason for it is that more flux leakage occurs and PM working point is decreasing at overload operation due to the bigger stator reluctance R_s. In view of this, the reason of the higher torque in the proposed hybrid rotor machines as shown in Fig. 1 (e)-(f) are that: on the one hand, there is a magnetic flux concentrated effect in spoke type part; on the other hand, surface-mount PM part plays an important role in a larger magnetomotive force, especially under high overload conditions.

Fig 12 shows the flux density distribution of rotor with different structures when the load current is 110A. It is observed that the magnetic flux leakage is the most serious in Fig 12 (e), followed by Fig 12 (b) and Fig 12 (c). This means that the size of the magnetic bridge has a very important influence on the peak torque. In addition, it also explains an advantage of SPM rotor under overload compared with the V type rotor as the relative value in Fig 10 (a) and (b).

C. COMPARISON OF PM EDDY LOSS AND EFFICIENCY

Fig. 13 shows the variations of the eddy current loss of the PM with the armature current ranged from 0A to 120A. It is obvious that the BHRPM machine has larger PM eddy current loss in four machines. Meanwhile, the V shape machine has maximum growth rate in PM eddy current loss. This is because that there is a large armature reaction because of a small equivalent air gap length compared with the SHRPM and BHRPM machines. Moreover, as shown in Fig. 13, the SHRSPM and SHRIPM represent the loss of the SHRPM machine in surface mount PM part and in spoke type PM part, respectively. The BHRSPM and BHRIPM are also the same meaning for the BHRPM machine. From the perspective of the loss distribution, the loss of the proposed hybrid machines in the surface mount part is majority which is exposed to the airs gap with large amount of harmonic content. For the proposed BHRPM machine, the suppression of the PM eddy

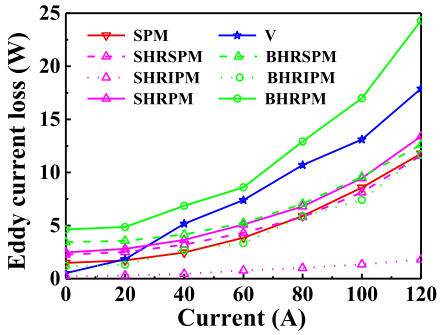

FIGURE 13. The variations of the eddy current loss with the current.

TABLE 3. The performance of machines with different rotor.

Items	SPM	VPM	SHRPM	BHRPM
Irated/ Ipeak (A)			20 / 110	
Trated (Nm)	7.65	7.75	8.45	8.75
Tpeak (Nm)	40.5	36.0	43.5	45.8
Overload multiple λ	5.29	4.65	5.15	5.23
Torque coefficient k_{20}	0.38	0.39	0.42	0.44
Torque coefficient k_{110}	0.37	0.33	0.40	0.42
Tripple (%)	6.0	4.6	3.0	11.2
P_{cu} (W)			88.2	
P_{Fe} (W)	15.64	14.03	18.5	18.68
P_{eddy} (W)	1.72	1.83	2.8	4.87
η	91.9%	92.1%	92.4%	92.6%
V_{pm} (10^{-6}m^3)	5.87	4.72	**5.8**	9.38
PM utilization	medium	high	medium	low

loss and the heat dissipation of the rotor are the content to be investigated further.

D. COMPARISON PERFORMANCE

As shown in Table 3, the main electromagnetic performance is compared with the conventional and proposed machines. Under limited space constraints of rotor, the proposed hybrid rotor machines have a larger average torque than SPM and VPM at rated and overload operation. However, each machine of the four type has own advantages. The SPM machine has a relatively big peak torque and is easy to be manufactured. The VIPM machine have a great PM utilization in spite of the weak overload capability. The SHRPM machine have a better performance in PM utilization due to less magnetic flux leakage than the BHRPM machine. But the manufacture and assembly are more complexity with non-magnetic connector and spliced rotor core. Above all, the choose of the two proposed machines can be determined according to the specific working conditions and economy.

V. EXPERIMENTAL VERIFICATION

The SHRPM rotor and SPM rotor machines are prototyped and partially prove the previous analysis. The total mass of machine is 4.6 kg including housing. The DC bus voltage is 160V. The maximum speed is 3000rpm. The experimental test platform is shown in Fig. 14. The digital controller is DSPACE 28335. The dynamic output torque is measured by a

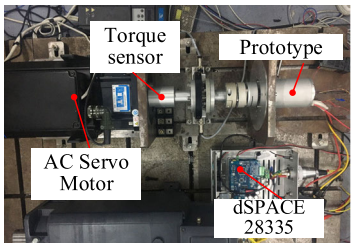

FIGURE 14. The experiment platform.

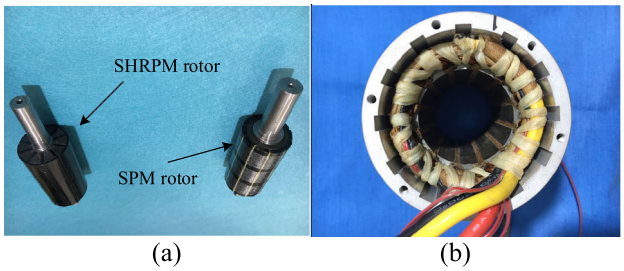

FIGURE 15. (a) SHRPM and SPM rotor (b) stator.

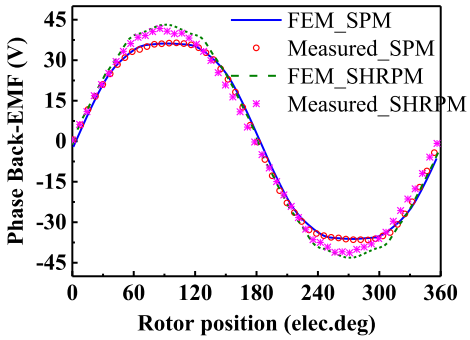

FIGURE 16. The comparison of the no-load phase back-EMF for SPM and SHRPM rotor machine.

TABLE 4. The comparisons of back EMF with different rotor between FEM and measured.

Items	Peak (V)		Fundamental wave amplitude (V)	
	FEM	Measured	FEM	Measured
SPM	36.86	36.3	40.18	39.5
SHRPM	43.1	41.6	44.0	42.1

torque transducer T40S2. Winding temperature is monitored by Applent instrument.

Two rotor structures are shown in the Fig. 15. The no-load back-EMF and torque in low load for SHRPM machine have been tested partially in [28]. Fig. 16 shows the comparison of FEM predicted and experiment measured. The parameters of peak and fundamental amplitude are shown in Table 4. The error of the fundamental amplitude for the SHRPM is 4.5%, however, the error of the SPM is 1.7%, this is because that the SHRPM machine is more complicated in rotor structure to be manufactured so that the error is relatively larger.

Fig 17 shows the speed and torque measured by experiment at the rated operating point for 4.5 min. The speed and torque

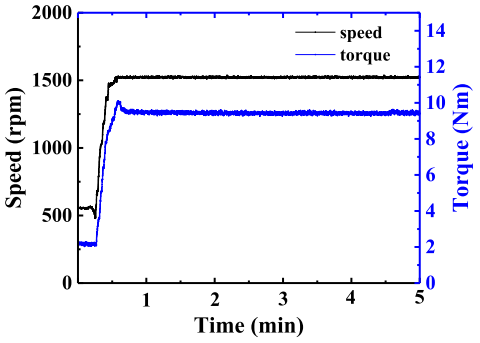

FIGURE 17. The speed and torque measured by experiment at the rated operating point.

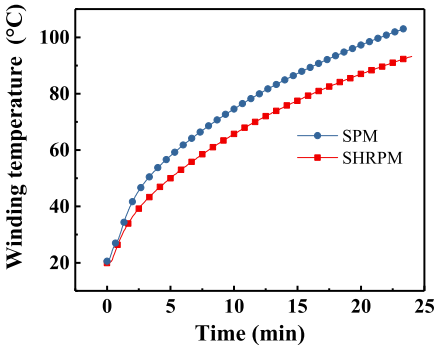

FIGURE 18. Three-phase winding temperature for SPM and SHRPM machine at rated operating point.

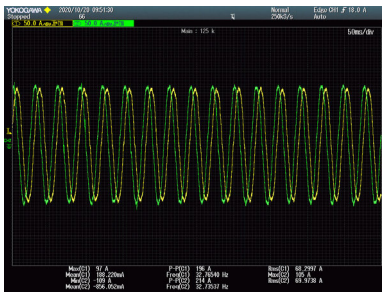

FIGURE 19. The Current waveform for SPM machine when the torque is 35Nm.

are 1500rpm and 9.5Nm, respectively, with the current rms 17.5A for SHRPM machine. The torque density is 2.1Nm/kg. The line load voltage is 83.2V and the phase load voltage is 45.4V. And the output power is 1.49 kw. The copper loss is 134.7W. The efficiency of machine is about 89.7%.

The temperature of winding for SHRPM is measured for 23 min as shown in Fig 18. The temperature is 92°C, which is not in a steady state. At the same time, the temperature of winding for SPM machine is 102°C with the same output torque as the SHRPM machine. This is a good performance that can withstand more than 20 minutes, and also has the ability to withstand short-term high overload.

Fig 19 shows the current waveform for SPM machine when the torque is 35Nm. From it, the root mean square (RMS) is 69.14A, which means that the current density is 50A/mm^2.

FIGURE 20. Three-phase winding temperature rise for SPM machine when the torque is 35Nm.

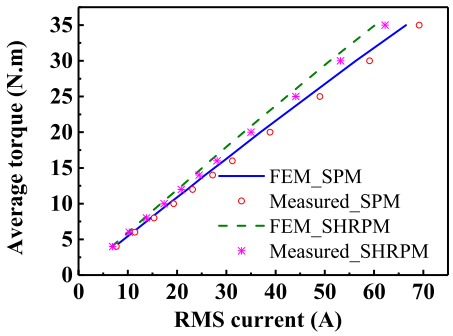

FIGURE 21. The comparisons of the torque with RMS current.

Fig 20 shows temperature rise of the three-phase winding. For short term high torque condition, temperature rises sharply in a short time that the maximum is 196°C. However, the temperature rise is different, this is because the temperature rise gradient of each part of the winding is larger, moreover, the relative positions measured by the temperature sensor are not exactly the same for the three phase windings.

Fig 21 shows the comparison of the torque with the FEM predicted and experiment measured. The x axis coordinates represent RMS current. By the error analysis, the torque error prediction by the FEM is 5.8% and 5.3% compared with the experiment measured, in SPM rotor and SHRPM rotor machines, respectively. The reason for the large torque prediction error compared with the no-load phase back-EMF is that there is a certain harmonic content in the output current of the drive.

VI. CONCLUSION

In this paper, in order to improve the torque density (rated torque density and peak torque density), four rotor structure machines are analyzed. First, the flux leakage and permanent magnet thickness is two key parameters for overload capacity of machines by the analysis of the core saturation effect. Then, the conventional and hybrid machines are optimized by the FEM. Interior PM machines with V type, V- type, U type and U- type rotor, are investigated. The result show that under the same current conditions, the peak torque can be larger although the rated torque may be relatively smaller. Finally, the electromagnetic performance is compared in open circuit flux density, torque, PM eddy current loss, etc. The

result shows that the SHRPM machine have a higher torque with growth rate 13.1%. The SPM rotor and SHRPM rotor machines is prototyped to validate the analysis.

REFERENCES

[1] G. Xu, G. Liu, W. Zhao, Q. Chen, and X. Du, "Principle of torque-angle approaching in a hybrid rotor permanent-magnet motor," *IEEE Trans. Ind. Electron.*, vol. 66, no. 4, pp. 2580–2591, Apr. 2019.

[2] C. López-Torres, A. Garcia, J.-R. Riba, G. Lux, and L. Romeral, "Computationally efficient design and optimization approach of PMa-SynRM in frequent operating torque–speed range," *IEEE Trans. Energy Convers.*, vol. 33, no. 4, pp. 1776–1786, Dec. 2018.

[3] W. Zhao, A. Ma, J. Ji, X. Chen, and T. Yao, "Multiobjective optimization of a double-side linear Vernier PM motor using response surface method and differential evolution," *IEEE Trans. Ind. Electron.*, vol. 67, no. 1, pp. 80–90, Jan. 2020.

[4] P. Arumugam and C. Gerada, "Short term duty electrical machines," in *Proc. ICEM*, Lausanne, Switzerland, 2016, pp. 2676–2681.

[5] Y.-X. Liu, L.-Y. Li, Q.-H. Gao, J.-W. Cao, R.-H. Wang, and Z.-Y. Sun, "Analytical model of torque-prediction for a novel hybrid rotor permanent magnet machines," *IEEE Access*, vol. 7, pp. 109528–109538, 2019.

[6] M.-J. Kim, S.-Y. Cho, K.-D. Lee, J.-J. Lee, J.-H. Han, T.-C. Jeong, W.-H. Kim, D.-H. Koo, and J. Lee, "Torque density elevation in concentrated winding interior PM synchronous motor with minimized magnet volume," *IEEE Trans. Magn.*, vol. 49, no. 7, pp. 3334–3337, Jul. 2013.

[7] A. M. EL-Refaie, J. P. Alexander, S. Galioto, P. B. Reddy, K.-K. Huh, P. de Bock, and X. Shen, "Advanced high-power-density interior permanent magnet motor for traction applications," *IEEE Trans. Ind. Appl.*, vol. 50, no. 5, pp. 3235–3248, Sep. 2014.

[8] M. Kimiabeigi, B. C. Mecrow, J. D. Widmer, R. Long, Y. Gao, J. Goss, R. Martin, T. Lisle, J. M. S. Vizan, and A. Michaelides, "On selection of rotor support material for a ferrite magnet spoke-type traction motor," *IEEE Trans. Ind. Appl.*, vol. 52, no. 3, pp. 2224–2233, May 2016.

[9] S.-I. Kim, J. Cho, S. Park, T. Park, and S. Lim, "Characteristics comparison of a conventional and modified spoke-type ferrite magnet motor for traction drives of low-speed electric vehicles," *IEEE Trans. Ind. Appl.*, vol. 49, no. 6, pp. 2516–2523, Nov. 2013.

[10] W. Kakihara, M. Takemoto, and S. Ogasawara, "Rotor structure in 50 kW spoke-type interior permanent magnet synchronous motor with ferrite permanent magnets for automotive applications," in *Proc. IEEE Energy Convers. Congr. Expo.*, Denver, CO, USA, Sep. 2013, pp. 606–613.

[11] M. Pourahmadi-Nakhli, A. Rahideh, and M. Mardaneh, "Analytical 2-D model of slotted brushless machines with cubic spoke-type permanent magnets," *IEEE Trans. Energy Convers.*, vol. 33, no. 1, pp. 373–382, Mar. 2018.

[12] P. Liang, F. Chai, L. Chen, and Y. Wang, "Analytical prediction of no-load stator iron losses in spoke-type permanent-magnet synchronous machines," *IEEE Trans. Energy Convers.*, vol. 33, no. 1, pp. 252–259, Mar. 2018.

[13] P. Liang, F. Chai, Y. Bi, Y. Pei, and S. Cheng, "Analytical model and design of spoke-type permanent-magnet machines accounting for saturation and nonlinearity of magnetic bridges," *J. Magn. Magn. Mater.*, vol. 417, pp. 389–396, Nov. 2016.

[14] P. Liang, F. Chai, Y. Yu, and L. Chen, "Analytical model of a spoke-type permanent magnet synchronous in-wheel motor with trapezoid magnet accounting for tooth saturation," *IEEE Trans. Ind. Electron.*, vol. 66, no. 2, pp. 1162–1171, Feb. 2019.

[15] K. Wang, Z. Q. Zhu, G. Ombach, and W. Chlebosz, "Average torque improvement of interior permanent-magnet machine using third harmonic in rotor shape," *IEEE Trans. Ind. Electron.*, vol. 61, no. 9, pp. 5047–5057, Sep. 2014, doi: 10.1109/TIE.2013.2286085.

[16] M. Si, X. Yu Yang, S. Wei Zhao, and S. Gong, "Design and analysis of a novel spoke-type permanent magnet synchronous motor," *IET Electr. Power Appl.*, vol. 10, no. 6, pp. 571–580, Jul. 2016.

[17] R. Y. Tang, "Permanent magnet synchronous generators," in *Modern Permanent Magnet Machines*. Beijing, China: CPM, 1997, ch. 8, pp. 273–292.

[18] D. Y. Kim, J. K. Nam, and G. H. Jang, "Reduction of magnetically induced vibration of a spoke-type IPM motor using magnetomechanical coupled analysis and optimization," *IEEE Trans. Magn.*, vol. 49, no. 9, pp. 5097–5105, Sep. 2013.

[19] Y. Demir and M. Aydin, "Design of a spoke type IPM synchronous motor with segmented rotor for low DC voltage applications," in *Proc. ECCE*, Pittsburgh, PA, USA, Sep. 2014, pp. 3556–3561.

[20] X. Ge, Z. Q. Zhu, J. B. Li, and J. T. Chen, "A spoke-type IPM machine with novel alternate airspace barriers and reduction of unipolar leakage flux by step-staggered rotor," in *Proc. IEEE Int. Electr. Mach. Drives Conf. (IEMDC)*, Coeur d'Alene, ID, USA, May 2015, pp. 53–59.

[21] J. Li, K. Wang, and C. Liu, "Comparative study of consequent-pole and hybrid-pole permanent magnet machines," *IEEE Trans. Energy Convers.*, vol. 34, no. 2, pp. 701–711, Jun. 2019.

[22] K. Wang, J. Li, S. S. Zhu, and C. Liu, "Novel hybrid-pole rotors for consequent-pole PM machines without unipolar leakage flux," *IEEE Trans. Ind. Electron.*, vol. 66, no. 9, pp. 6811–6823, Sep. 2019.

[23] Y. Hu, S. Zhu, C. Liu, and K. Wang, "Electromagnetic performance analysis of interior PM machines for electric vehicle applications," *IEEE Trans. Energy Convers.*, vol. 33, no. 1, pp. 199–208, Mar. 2018.

[24] P. B. Reddy, A. M. El-Refaie, K.-K. Huh, J. K. Tangudu, and T. M. Jahns, "Comparison of interior and surface PM machines equipped with fractional-slot concentrated windings for hybrid traction applications," *IEEE Trans. Energy Convers.*, vol. 27, no. 3, pp. 593–602, Sep. 2012.

[25] P. M. Wensing, A. Wang, S. Seok, D. Otten, J. Lang, and S. Kim, "Proprioceptive actuator design in the MIT cheetah: Impact mitigation and high-bandwidth physical interaction for dynamic legged robots," *IEEE Trans. Robot.*, vol. 33, no. 3, pp. 509–522, Jun. 2017.

[26] S. Seok, A. Wang, M. Y. Chuah, D. J. Hyun, J. Lee, D. M. Otten, J. H. Lang, and S. Kim, "Design principles for energy-efficient legged locomotion and implementation on the MIT cheetah robot," *IEEE/ASME Trans. Mechatronics*, vol. 20, no. 3, pp. 1117–1129, Jun. 2015.

[27] S. Seok, A. Wang, M. Y. Chuah, D. Otten, J. Lang, and S. Kim, "Design principles for highly efficient quadrupeds and implementation on the MIT cheetah robot," in *Proc. IEEE Int. Conf. Robot. Automat.*, Karlsruhe, Germany, May 2013, pp. 3307–3312.

[28] Y. Liu, L. Li, Q. Gao, J. Cao, and Z. Sun, "An analytical model and optimization of a novel hybrid rotor machine for high torque density," *IEEE Trans. Energy Convers.*, early access, Jul. 13, 2020, doi: 10.1109/TEC.2020.3008768.

YU-XI LIU was born in Hunan, China. He received the B.E. and M.E. degrees in electrical engineering from the Xi'an Research Institute of High Technology, Xi'an, China, in 2014 and 2017. He is currently pursuing the Ph.D. degree with the School of Xi'an Research Institute of High Technology.

His current research interest includes design of high-power/torque density permanent magnetic machines.

JI-WEI CAO (Member, IEEE) received the B.E. and M.E. degrees in electrical engineering from the Shenyang University of Technology (SUT), Shenyang, China, in 2005 and 2008, respectively, and the D.E. degree in electrical engineering from the Harbin Institute of Technology (HIT), Harbin, China, in 2014.

He is currently with the Institute of Electromagnetic and Electronic Technology, HIT. His research interest includes development and improvement of power density for the effective design of electric motor.

QIN-HE GAO received the B.E., M.E., and D.E. degrees from the Xi'an High-Tech Institution, Xi'an, China, in 1989, 1993, and 2002, respectively.

Since 2010, he has been a Professor with the School of the Institute of Armament Science and Technology, Xi'an High-Tech Institution. His research interests include electro-hydraulic system simulation and electromechanical control technology.

ZHI-HAO LIU received the B.E., M.E., and D.E. degrees in mechanical engineering from the Xi'an Research Institute of High Technology, Xi'an, China, in 2011, 2013, and 2018, respectively. He is currently an Associate Professor with the Institute of Armament Launch Theory and Technology, Xi'an Research Institute of High Technology. His research interests include non-linear dynamics and intelligent application of the high speed ride comforty.

YA-CHAO LU received the B.E. degree from the Xi'an High-Tech Institution, Xi'an, China, in 2014. He is currently with the Xi'an Institute of Optics and Precision Mechanics of CAS. His research interest includes development of mechanical design.

ZHI-YIN SUN (Member, IEEE) received the B.E., M.E., and D.E. degrees in electrical engineering from the Harbin Institute of Technology (HIT), in 2009, 2011, and 2016, respectively.

From 2014 to 2015, she was a Joint Training Ph.D. Student with Physikalisch-Technische Bundesanstalt, Germany, working on precise magnetic field analysis. She is currently a Research Associate with the Laboratory for Space Environment and Physical Sciences, HIT. She is also holding a postdoctoral position with the Helmholtz-Institute Mainz, Germany. Her research interests include electrical machines, weak magnetic field realization, and ultra-sensitive measurement. She was awarded a scholarship under the International Postdoctoral Exchange Fellowship Program 2017.